ACS APPLIED MATERIALS & INTERFACES

Research Article

www.acsami.org

Nanoparticle Flotation Collectors—The Influence of Particle Softness

Songtao Yang,[†] Bi Bi Marzieh Razavizadeh,[‡] Robert Pelton,*[,†] and Gerard Bruin[†]

[†]Department of Chemical Engineering, McMaster University, 1280 Main Street West, Hamilton, Ontario, Canada L8S 4L7

[‡]Research Institute of Food Science and Technology, P.O. Box 91735-147, Mashhad, Iran

Supporting Information

ABSTRACT: The ability of polymeric nanoparticles to promote glass bead and pentlandite (Pn, nickel sulfide mineral) attachment to air bubbles in flotation was measured as a function of the nanoparticle glass transition temperature using six types of nanoparticles based on styrene/N-butylacrylate copolymers. Nanoparticle size, surface charge density, and hydrophobicity were approximately constant over the series. The ability of the nanoparticles to promote air bubble attachment and perform as flotation collectors was significantly greater for softer nanoparticles. We propose that softer nanoparticles were more firmly attached to the glass beads or mineral surface because the softer particles had a greater glass/polymer contact areas and thus stronger overall adhesion. The diameters of the contact areas between polymeric nanoparticles and glass surfaces were estimated with the Young−Laplace equation for soft, liquidlike particles, whereas JKR adhesion theory was applied to the harder polystyrene particles. The diameters of the contact areas were estimated to be more than an order of magnitude greater for the soft particles compared to harder polystyrene particles.

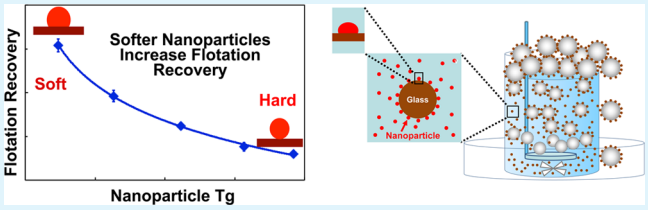

KEYWORDS: *mineral flotation, flotation collectors, nanoparticle Tg, contact angle, adhesion, pentlandite*

INTRODUCTION

Froth flotation is a critical operation in most mineral processing operations.[1] In this technology, ores are ground to give aqueous slurries consisting of ∼100 μm diameter particles. To isolate valuable mineral-rich particles from the many unwanted "gangue" particles, the suspension is treated with a "collector chemical" that selectively renders the desired particle surfaces sufficiently hydrophobic so that the desired particles can be isolated by passing air bubbles through the suspension. The more hydrophobic mineral particles adhere to air bubbles, and rise to the froth phase for easy separation. Recently we have shown that hydrophobic polymeric nanoparticles (latex) can function as flotation collectors and may offer advantages over traditional surfactant collectors.[2−4] The use of polymeric latexes in mineral processing is not new. Following some work from the USSR translated in 1979,[5] theses[6,7] and publications have described the use of latex to flocculate fine coal particles.[8−12] Although most of these studies did not involve flotation, Zhan's thesis reported apatite flotation in the presence of poly(methyl acrylate-co-acrylic acid) copolymer latex, with and without an oleic acid collector.[6]

To develop nanoparticle design rules for this application, we have designed model flotation experiments involving glass beads as a mineral surrogate, and cationic latex particles as nanoparticles. This simple experimental system has allowed us to show the influence of nanoparticle size, coverage, and hydrophobicity. For glass bead flotation, 46 nm nanoparticles were better collectors than larger nanoparticles,[4] with the best cases giving excellent flotation with as little as 5% of the glass bead surfaces covered with adsorbed nanoparticles. For an ore containing 1.4 wt % pentlandite with a specific surface area of 0.076 m^2/g (measured value for first concentrate), a "best case" 5% area coverage corresponds to 1.7 g of nanoparticles per tonne of ore, suggesting that effective polymer nanoparticles could be commercially viable. In addition to flotation experiments, we used micromechanics measurements to determine pull-off forces for glass beads adhering to air bubbles as functions of nanoparticle properties.[2]

Herein, we explore the role of nanoparticle softness. For this, a series of monodisperse polymer nanoparticles was prepared with varying glass transition temperatures but with near constant size, surface charge and water contact angles. Surprisingly, the results herein show that softer particles were superior flotation collectors.

EXPERIMENTAL SECTION

Materials. Styrene (99%, Sigma-Aldrich) and butyl acrylate (≥99%, Sigma-Aldrich) were passed through inhibitor-removing columns. 2,2′-Azobis (2-methylpropionamidine) dihydrochloride (V50, 97%) and poly(allylamine hydrochloride) (PAAm, M_w ∼ 15 KDa) was purchased from Sigma-Aldrich and used as supplied. Polyvinylamine (PVAm) solution, LUPAMIN 1595 (M_w ≈ 10 kDa) was donated by BASF (Ludwigshafen, Germany) and was purified via dialysis. The frother, UNIFROTH 250C (99%) was donated by Vale Canada (Mississauga, ON). Glass beads (30−50 μm) were purchased from Polysciences, Inc. Glass beads, unwashed (≤106 μm, −140 U.S. sieve) were purchased from Sigma-Aldrich. Particle size distributions

Received: February 11, 2013
Accepted: May 21, 2013
Published: May 21, 2013

for the two beads used in flotation have been given in the Supporting Information. The surface weighted mean diameter (Sauter mean diameter, D_{32}) is 43 μm for 30−50 μm glass beads and 66 μm for the ≤106 μm ones.[4] All solutions were made with Type 1 water (18.2 MΩcm, Barnstead Nanopure Diamond system).

High-grade pentlandite ($Ni_{4.5}Fe_{4.5}S_8$, Pn) was provided by Vale. The high-grade Pn from Vale was prepared as following. A Cu rougher tails sample taken from the Cu/Ni separation circuit at Clarabelle Mill was further purified in the Minerals lab at Vale. The purification included: a) chalcopyrite (Cp) flotation took place at high pH, ∼12.0, with prolonged aeration time, i.e., 30 min; (b) the flotation tails underwent further flotation using Aero 3418A to float Cp followed by using PAX to float pyrrhotite (Po). The Po flotation tails is the purified Pn. The Pn sample had a nickel content of 27 ± 2%. Note the Ni grade of 100% pure pentlandite, $Ni_{4.5}Fe_{4.5}S_8$, is about 34%. Pn was chemically cleaned with a Vale standard procedure, to remove residual xanthate and oxidation products from surfaces. Five g Pn and 50 mL of deoxygenated 0.1 M HCl were mixed in a three-necked 100 mL flask equipped with a condenser, a rubber stopper with a needle valve for N_2 purging, and a magnetic stirring bar. The mixtures were mixed for 1 h followed by settling and decanting the supernatant. The sediment was twice washed with 50−80 mL deoxygenated water. Fifty milliliters of deoxygenated 0.5 M $Na_2S{\cdot}9H_2O$ solution were added, and the suspension was mixed at room temperature for 5 h. After rinsing and decantation twice with 75 mL of deoxygenated water, the suspensions were diluted with deoxygenated water to give ∼0.1 g/mL suspensions used for flotation. The particle size distribution was measured with a Malvern Mastersizer 2000 giving a 12 μm surface weighted mean (Sauter mean diameter, D_{32}) particle size − the particle distribution is given in the Supporting Information. The electrophoretic mobility of Pn was −1.79 (±0.14) × 10^{-8} m^2 s^{-1} V^{-1} (pH 7.0).

Ultramafic low-grade (∼ 0.47%) nickel sulfide ore was obtained from the Pipe deposit of Thompson nickel belt, Manitoba Canada. The ore was crushed to −6 mesh (<3.36 mm) before primary grinding. The major valuable mineral is pentlandite, associated with iron sulfide mineral (pyrrhotite, $Fe_{1-x}S$, and pyrite, FeS_2, etc.), and large amounts of gangue materials (predominantly serpentine, $(MgFe)_3Si_2O_5(OH)_4$).

Nanoparticle Preparation and Characterization. The polymerizations for a series of poly(styrene-co-n-butylacrylate) (St-nBA) nanoparticles were conducted in a 250 mL three-necked flask equipped with a condenser, a glass stirring rod with a Teflon paddle, and a rubber stopper holding a syringe needle for nitrogen purging. Six types of nanoparticles were prepared by surfactant-free emulsion polymerization and the nanoparticle properties are summarized in Table 1.[13] For example for NP4, 100 mL of deionized water were charged to the reactor followed by nitrogen bubbling for 30 min at 70 °C with 200 rpm stirring. To the reactor were added 3.5 g of styrene and 2.3 g of butyl acrylate. The mixture was equilibrated for several minutes before 0.042 g of V50 dissolved in 10 mL of water was added to initiate the polymerization. The reaction was stirred at 70 °C for a total of 23 h. The resulting latex was dialyzed for 1 week against deionized water before further characterization or for use as a flotation collector.

Table 1. Nanoparticle Compositions and Properties[a]

nanoparticle designation	styrene (wt %)	electrophoretic mobility (× 10^{-8} m^2 s^{-1} V^{-1})	diameter (nm)	T_g (°C)
NP1	100	3.11 ± 0.15	255 ± 12	115
NP2	89	3.00 ± 0.10	271 ± 36	94
NP3	78	3.02 ± 0.16	273 ± 32	67
NP4	60	2.84 ± 0.25	233 ± 28	38
NP5	46	2.87 ± 0.19	223 ± 29	14
NP6	29	2.93 ± 0.21	254 ± 30	−2.2

[a]Styrene formed "hard" segments whereas the monomer, N-butylacrylate formed soft segments. The errors for the reported EM values were estimated from the average of 10 runs with each consisting of 15 scans. The errors for the nanoparticle diameters were calculated from the average of three time measurements.

Glass transition temperatures, T_g, of freeze-dried nanoparticles were measured with a modulated DSC instrument (TA Instruments, US). Nanoparticle hydrodynamic diameters were determined by dynamic light scattering (Brookhaven Instruments Corporation, BIC) using a detector angle of 90°. Correlation data were analyzed by BIC dynamic light scattering software (Windows 9KDLSW Version 3.34) using the cumulant model and the scattering intensity was set between 150 and 250 kcounts/s for each measurement. The duration for each measurement was set to 5 min. Electrophoretic mobility (EM) measurements were performed by a Zeta PALS instrument (Brookhaven Instruments Corp.) at 25 °C in phase analysis light scattering mode. The reported EM values were the average of 10 runs with each consisting of 15 scans. Samples for both dynamic light scattering and electrophoretic mobility measurements were prepared in clean vials by dispersing approximately 0.2 g/L of the nanoparticles in 5 mM NaCl.

Two nanoparticles (NP4 and NP5) were selected as the collectors for the low-grade ultramafic nickel ore. Before the flotation, NP4 was preadsorbed with 0.1 mg/m^2 PAAm and NP5 was pretreated with 0.075 mg/m^2 PVAm and were equilibrated overnight.

Flotation. In a typical flotation experiment, 2 g of 43 μm glass beads and 0.5 mL of nanoparticles (36 g/L for NP4) were added into 125 mL of 5 mM NaCl in a 150 mL plastic flotation beaker, sitting on a 90 mm diameter plastic Petri dish, which in turn was sitting on a magnetic stirrer (Corning Stirrer, model PC-610). Photographs of the apparatus are given in the Supporting Information.

The suspension of glass beads and nanoparticle dispersions was mixed for 5 min (25 mm ×25 mm cross-shape stirring bar at ∼600 rpm) to permit the nanoparticles to deposit onto the glass beads. Following conditioning, 0.12 mL of 1% UNIFROTH 250C (10 ppm) was added and mixed for an additional 30 s. Flotation was commenced by initiating nitrogen flow (Matheson 604 E700 Flow Controller) at a rate of 2.0 L/min through a Corning Pyrex gas dispersion tube (Fisher Scientific, 11−137E) consisting of a 30 mm coarse glass frit attached by a 90 degree elbow. During flotation the stirring rate was increased to ∼900 rpm to avoid bead sedimentation. The froth phase was scraped over the edge of the beaker and collected in the plastic Petri dish. After 1.0−1.5 min the gas flow was stopped and the plastic collection dish containing both liquid and beads was weighed; the beads were filtered through a Büchner funnel, dried, and weighed. Typically, each dish contained 50−60 mL of flotation liquor. The flotation results were expressed as the recovery, the mass fraction of beads that was recovered with the froth.

The extent of nanoparticle deposition on the glass beads was determined by measuring the absorbance of the supernatant nanoparticle dispersion at 500 nm (Beckman Coulter, DU800) before and after deposition (usually 7 min). The quantity of deposited latex was calculated using a calibration curve of absorbance versus nanoparticle concentration.

Flotation tests using the ultramafic nickel ore were performed in a 4.2 L Denver flotation cell. The tests were conducted according to Vale's standard incremental flotation procedure for the ultramafic ore as following.[14] One kilogram of the crushed −6 mesh (<3.36 mm) sample was ground in a laboratory rod mill in the presence of flotation process water (prepared with NaCl, pH 8.5) until 80% (by mass) of the particles were smaller than 106 μm. The ground slurry was then subjected to a desliming process using a Mozley 1 in. hydrocyclone to lower the slurry viscosity for flotation. The cyclone underflow (flotation feed) was charged into the flotation cell for the flotation test according to an incremental rougher flotation procedure that contains eight incremental flotation stages. In the conditioning step, the collector was added for 5 more minutes of conditioning before each incremental flotation, and the frother (20 ppm UNIFROTHER 250C) was added at 30 s before the start of each incremental flotation. Every flotation test was performed with the collection of eight incremental froth products for a total of 16 min, i.e., 2 min for each incremental flotation stage.

Each of the flotation products (concentrates, tails, and slime) was dried and weighed and the cumulative mass balance was 100 ± 0.25 wt % of the starting 1.0 kg ultramafic ore. The Ni content (grade) of the dried solids was measured by a Varian Vista inductively coupled plasma-optical emission spectrophotometer (ICP-OES).[15] The flotation results were plotted as curves of cumulative Ni grade as functions of cumulative Ni recovery, which was determined from mass balance of the flotation products.

Contact Angle Measurements. Contact angle measurements (for both sessile water drop methods and attached bubble methods) were performed on glass microscope slides (Gold Line Microscope Slides, VWR), which we assumed had similar surface characteristics to those of the glass beads. Typically, glass microscope slides were cut to approximately 9 mm squares, cleaned (Sparkleen detergent, Fisher Scientific), and immersed in 500−1000 mg/L (500 mg/L for NP4) nanoparticle suspension in 5 mM NaCl for times ranging from 30 to 60 min. The treated slides were then immersed in approximately 1 L of water to remove unbound nanoparticles. To prepare smooth polymer films for water contact angle measurements, dried nanoparticles were dissolved in THF (tetrahydrofuran, Certified, Fisher Scientific) and were spin coated on glass with a SPIN 150 Wafer Spinner running at 3000 rpm. Usually two glass slides were prepared for each condition. One slide was used to measure contact angles while the second one was used to obtain SEM images.

The contact angle measurements were performed using a Krüss contact angle measuring instrument running Drop Shape Analysis (DSA) 1.80.0.2 software. Three types of contact angle were measured. Advancing water contact angles were recorded by forming a water drop on the end of a fine glass capillary tube (the tip diameter ∼40−50 μm) and pushing the drop to contact with either an air-dried latex treated glass slide (θ_a) or a smooth polymer film (θ_{sa}). Attached bubble receding contact angle (θ_r) was acquired by forming an air bubble from the capillary and slowly pushing the air bubble in contact with never-dried treated glass slides that immersed in water, transferring the bubble to the surface, yielding a receding contact angle. More details of the methodology have been published recently.[3]

The images of the attached air bubble profiles on the never-dried treated glass slides were captured with the Krüss contact angle instrument camera. The receding contact angles were the average of manual measurements on three bubbles using the Image J 1.45s angle tool. The diameters of attached bubbles were measured with ImageJ 1.45s pixel converter. The pixel dimensions were calibrated with a 1 mm (0.01 mm ×100) quartz calibration ruler.

Electron Microscopy. Nanoparticle distributions on the dried nanoparticle treated glass slides were investigated by using a JEOL JSM-7000F scanning electron microscope (SEM).

RESULTS

Six types of polymeric nanoparticles were prepared by surfactant free batch polymerization of styrene and N-butylacrylate and the compositions and properties are summarized in Table 1. Styrene gives a hard polymer with a high glass transition temperature, whereas poly(N-butylacrylate) is a soft polymer. The nanoparticle dispersions had narrow particle size distributions and were approximately the same size over the series. The nanoparticles were positively charged because of the presence of surface amidine groups from the cationic free radical polymerization initiator.[13] The positive charge facilitated the spontaneous adsorption of nanoparticles onto glass beads, pentlandite, and glass slides.

The role of nanoparticle flotation collectors is to facilitate mineral particle attachment to air bubbles. Contact angle measurements and bubble attachment experiments were performed on flat glass surfaces. Hydrophilic glass surfaces decorated with hydrophobic nanoparticles show complex behaviors. In earlier work,[3] we developed three types of contact angle measurements for this system:

1. Advancing contact angles, θ_a, in which nanoparticles are adsorbed on glass slides, the slides are dried, and a conventional advancing angle measurement is made with a water drop. Receding measurements are not possible with this geometry because of extreme pinning.
2. Receding contact angles, θ_r, were measured by attaching air bubbles to nanoparticle treated glass slides. In these experiments the nanoparticle treated slides were never dried, a situation closest to flotation. Previous work with polystyrene (i.e., hard) nanoparticles showed that high flotation yields correspond to receding contact angles greater than 25°.
3. Polymer contact angles, θ_{sa}, in which the nanoparticles were dissolved in a solvent and cast in a smooth film on glass. Conventional advancing water contact angles gave a measure of the polymer hydrophobicity, assuming that the smooth cast polymer films had the same surface chemistry as the parent nanoparticles. The advancing and receding angles on the smooth polymer films were very similar as expected for smooth films.

The three types of contact angle measurements were performed with each of six types of nanoparticles of varying hardness, and the results are summarized in Figure 1 as

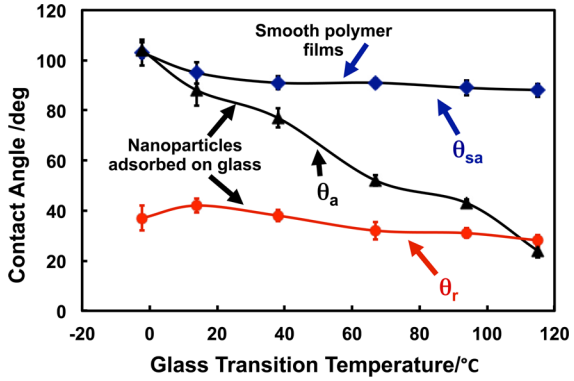

Figure 1. Three types of contact angles for 6 types of nanoparticles. The surfaces were either glass slides saturated with adsorbed nanoparticles or smooth polymer films cast from solution. The nanoparticles corresponding to the glass transition values are given in Table 1. The error bars are calculated from three measurements on different positions of the treated slides.

functions of the nanoparticle glass transition temperatures. In these experiments the glass surfaces had a saturated coating of adsorbed nanoparticles. The conventional advancing contact angles showed the largest range of values over the series, with the softer particles (i.e., the lower T_g values) giving the highest angles. Because the nanoparticle-treated slides were air-dried before the measurements, the softer nanoparticles were able to spread, filling in hydrophilic voids between the particles. Figure 2 shows electron micrographs of glass surfaces treated with the 6 nanoparticle types. NP1−3 appear as spheres on a surface, NP4 shows significant coalescence, and NP5−6 appear as homogeneous films.

The highest series of contact angle measurements was the advancing water contact angles for the smooth films, θ_{sa}. These measurements reflect the hydrophobicity of the nanoparticle surfaces. The contact angles were nearly independent of composition, suggesting that the hydrophobicity was approximately constant over the series. Note that for the lowest two

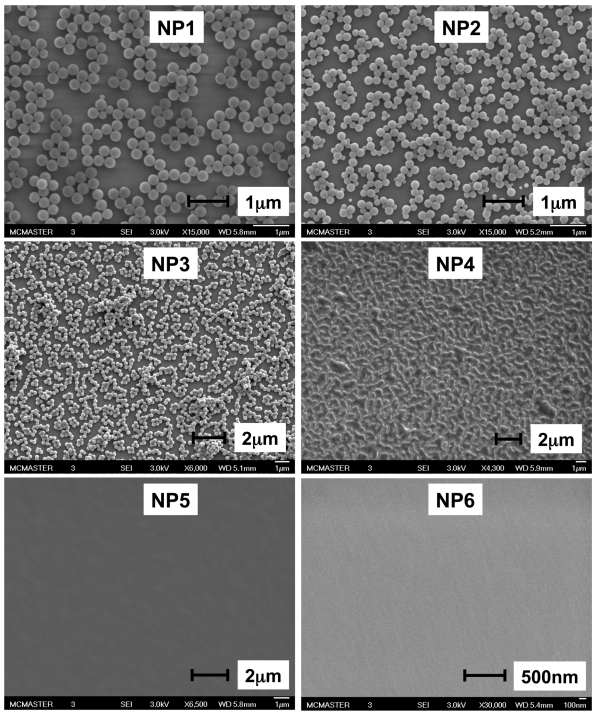

Figure 2. SEM images of glass slide surfaces with a saturated coating of adsorbed nanoparticles. The softest particles coalesced into smooth films after drying.

T_g values the contact angles were nearly equal for the cast films, θ_{sa}, and for the dried treated glass slides, θ_a.

Receding contact angles, θ_r, are the most relevant contact angles for flotation because with bubble attachment to a submerged surface, the three phase contact line forms on previously wetted surfaces. The results in Figure 1 showed that all of the values fell within the narrow range of 28−42°. Therefore, we propose that in analyzing the influence of nanoparticle softness on flotation, the series of nanoparticles in Table 1 has similar surface energies, and thus other explanations for softness effects are required.

Small-scale laboratory flotation experiments were conducted and Figure 3 summarizes the results for the six nanoparticles with glass beads and with a cleaned pentlandite (Pn, nickel mineral) suspension. Flotation performance was measured as the "recovery", defined as the mass fraction of added beads isolated with the froth after a fixed flotation time. For these experiments, the nanoparticle concentration was high enough to coat up to 85% ± 10% bead surface area. Clearly flotation efficiency was very sensitive to the nanoparticle T_g, with NP5 giving the maximum recovery. Both glass bead and Pn suspensions gave similar results.

When measuring the receding contact angles, we also measured the maximum diameter of the bubbles that could attach to the nanoparticle coated glass slides in water, and the results are shown in Figure 4. Flotation recovery was a linear function of the maximum attached bubble diameter. However, NP6, the lowest T_g nanoparticle seemed to be an outlier.

All the results so far presented have involved high coverages of nanoparticles on the beads or glass slides. The practical application of nanoparticle flotation collectors requires that they function at low coverages. Figure 5 shows bead recovery as functions of the bead surface areas covered with nanoparticles.

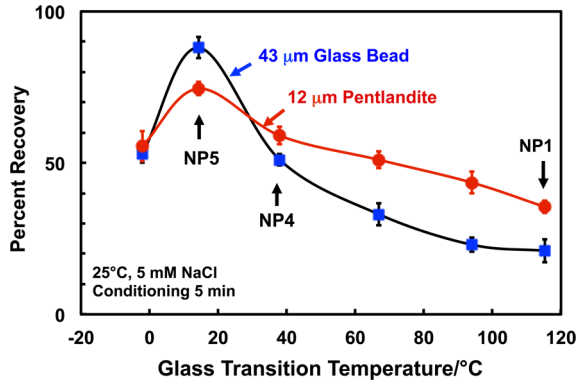

Figure 3. Percentage of added glass beads or cleaned pentlandite (Pn) recovered by flotation as a function of the nanoparticle glass transition temperature. Nanoparticle dosage was high enough to coat 85 ± 10% of the bead and Pn surfaces. With no collector addition, the glass bead recovery was 4% and the Pn recovery was 22%. The pH values for the glass bead and Pn experiments were 6.7 ± 0.4 and 8.4 ± 0.6, respectively. The error bars for the glass bead results were based on the mass balance, whereas the bars on the Pn results reflect the range of duplicated experiments.

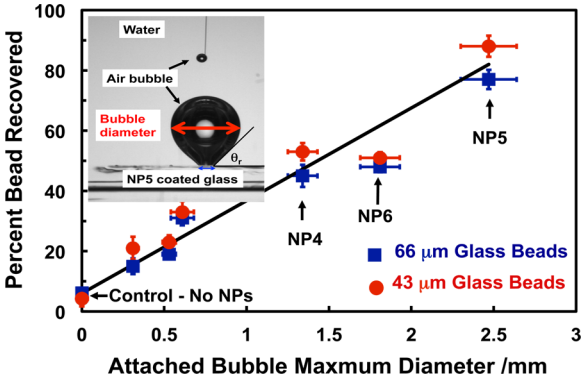

Figure 4. Glass bead recovery in flotation as functions of the maximum bubble diameter that could be supported on glass slides treated with nanoparticles. The horizontal error bars reflect the range of triplicate measurements; the vertical bars were estimated from the mass balance of the flotation streams.

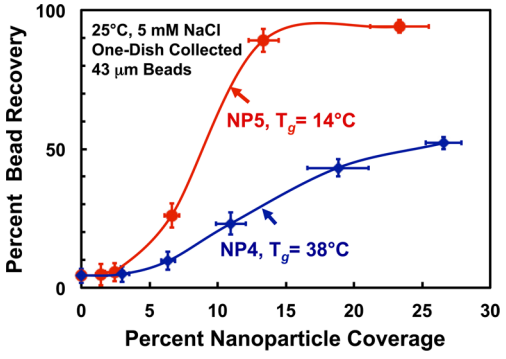

Figure 5. Glass bead recovery as functions of coverage, the percentage of the glass bead surface covered with nanoparticles.

NP5 was much more effective than NP4, giving a high maximum recovery with less than 15% coverage.

Finally, to demonstrate that our results are relevant to commercial flotation operations, we performed flotation experiments with NP4 and NP5 nanoparticle flotation

dx.doi.org/10.1021/am4008825 | ACS Appl. Mater. Interfaces 2013, 5, 4836−4842

collectors in Thompson Pipe, a difficult-to-separate ultramafic ore. Figure 6 shows the nickel grade, a measure of the purity of

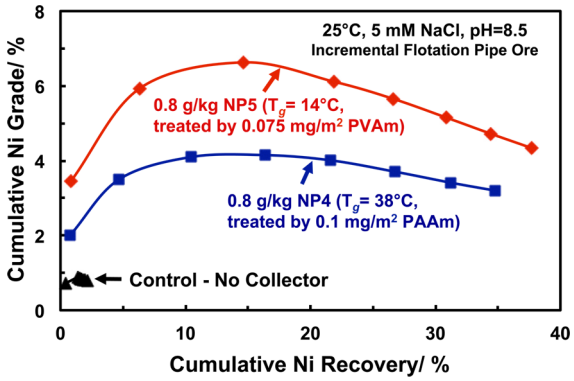

Figure 6. Influence of nanoparticle softness on the flotation behavior of an ultramafic nickel ore. The nanoparticles were treated with polyvinylamine to increase the affinity to Pn. By commercial standards, both collectors are poor; however, the softer NP5 is superior.

the separated mineral, versus percent recovery, a measure of the yield of the collected mineral. By commercial standards, both maximum grade and recoveries are low for both nanoparticles. However, the results again indicate that the softer NP5 is more effective than NP4, which has a high T_g. Note that in these experiments, the nanoparticles were pretreated with polyvinylamine, a nickel chelating polymer, in an effort to facilitate the selective interaction with pentlandite.

In summary, this series of nanoparticles shows a strong sensitivity to the glass transition temperature of the nanoparticles where the particle size, surface charge, and intrinsic hydrophobicity was approximately constant. Why?

DISCUSSION

The role of the nanoparticles in our experiments was to facilitate the attachment of glass beads (model for mineral particles) to air bubbles. Nuguyen et al. argued that the attachment step involves three processes: (1) thinning of the intervening water film between the mineral particle and the bubble; (2) rupture of the film to give a three-phase "contact nucleus"; and (3) expansion of the three-phase-contact-line (TPCL) from the critical radius to form a stable wetting perimeter.[16] Nanoparticle softness should not influence process (1), thinning of the water film between a glass bead and an air bubble. Similarly, there is no mechanism we know of that predicts softer particles will promote step (2), the initial film rupture. Indeed the contrary is true; in defoamer technology, hydrophobic particles are used to nucleate foam film rupture and hard, hydrophobic particles with asperities would be more effective than smooth, soft particles.[17−19] Therefore, we believe that expansion of the three phase contact line is the air bubble attachment step most impacted by nanoparticle softness. Specifically, we propose that softer particles perform better because they are more firmly attached to the glass surface. Adhesion is important because nanoparticles weakly attached to the glass beads could be removed by transfer to air bubbles or could move across the glass/water interface, lowering the probability of air bubble attachment to the beads.

The influence of nanoparticle softness on the adhesion to surfaces has been considered in a number of publications.[20−23] Herein softness effects are illustrated by applying standard adhesion theories to two cases: (A) a liquid polymer droplet adhering to glass; and (B) a polystyrene sphere adhering to glass. The equilibrium contact diameters can be estimated as follows. For a liquid polymer drop on a glass surface immersed in water, the contact angle is given by the Young−Laplace equation where γ_{gw} is the surface energy of the glass/water interface, γ_{pw} is the interfacial energy of the polymer/water interface, γ_{gp} is the glass/polymer interfacial energy, and $\theta$is contact angle the liquid polymer drop makes with a glass surface under water.

$$\gamma_{gw} = \gamma_{gp} + \gamma_{pw}\cos(\theta) \tag{1}$$

The corresponding work of adhesion between the liquid polymer and glass in water is given by the following classical expression.

$$W_a = \gamma_{pw}(1 - \cos(\theta)) \tag{2}$$

If we assume a spherical drop shape, the following expression gives the diameter of the contact patch, D_Y between the liquid polymer and the glass where r_{np} is the radius of the original liquid sphere before contacting the surface.

$$D_Y = 4\sqrt[3]{\frac{r^3}{\frac{1-\cos(\theta)}{\sqrt{1-\cos(\theta)^2}}\left(3 + \frac{1-\cos(\theta)}{1+\cos(\theta)}\right)}} \tag{3}$$

The liquid polymer contact diameter, D_Y, was calculated as a function of the work of adhesion using eqs 2 and 3. The resulting curve for γ_{pw} = 30 mN/m[24] is shown as the red curve in Figure 7.

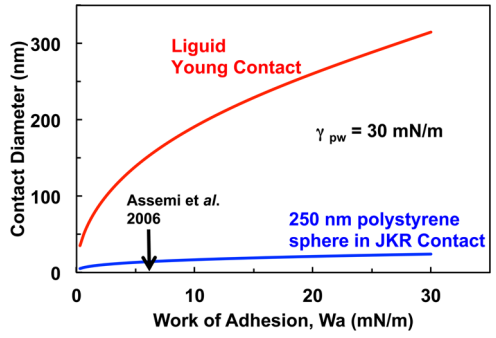

Figure 7. Comparing the contact patch diameter for a polystyrene 250 nm nanoparticle on glass in water to the corresponding liquid polymer as functions of the polymer/water/glass work of adhesion.

JKR theory,[25,26] was used to estimate the corresponding contact patch diameter, D_{JKR} for harder polystyrene particles as a function of the work of adhesion. The following equation applies to a sphere on a plate with no applied pressure where: ν = 0.35 is Poisson's ratio for polystyrene; E = 3.3 GPa is Young's modulus for polystyrene; and as above, W_a is the work of adhesion.

$$D_{JKR} = 2\left[6\pi W_a r^2\left(\frac{3}{4}\frac{1-\nu^2}{E}\right)\right]^{1/3} \tag{4}$$

If the liquid polymer droplet has the same work of adhesion to glass in water as polystyrene, the calculations in Figure 7 predict that the contact patch diameter of the liquid drop on glass is about an order of magnitude greater than for the polystyrene particle with the same surface energies. Assuming pull-off forces

dx.doi.org/10.1021/am4008825 | ACS Appl. Mater. Interfaces 2013, 5, 4836−4842

scale with the contact circumference, the Young−Laplace liquid contacts have a much greater detachment force. Summarizing, we propose that the nanoparticles in Table 1 fall within the extremes shown in Figure 7. NP1 is pure polystyrene and should be described by the JKR contact line, whereas NP5−6 with low T_g values should behave more like the Young contact case. Assemi et al. in a study of polystyrene latex adhesion to glass in water, estimated that the work of adhesion was 6.4 mN/m, shown as the arrow in Figure 7.[27] The corresponding Young contact diameter is 156 nm, whereas the JKR diameter is only 14 nm.

NP6, the lowest T_g nanoparticle type, was not as effective as the harder NP5 for both glass beads and cleaned Pn - we are not sure why. The receding contact angles (θ_r) curve in Figure 1 showed a slight maximum corresponding to NP5, perhaps indicating that NP6 was slightly less hydrophobic than NP5.

Ongoing efforts in our laboratory are focused on the design of nanoparticles for mineral flotation. The results herein suggest that softness of the core particle is important. Nevertheless, our current generation of nanoparticle flotation collectors is far less efficient in commercial mineral suspensions compared to the theoretical best case of a few grams of nanoparticle per tonne of ore, an estimate based on flotation results with model glass bead flotation experiments. Ideal nanoparticle flotation collectors must be colloidally stable in the flotation solution, specifically deposit onto mineral-rich surfaces, and must be sufficiently hydrophobic to promote mineral/air bubble adhesion. The nanoparticle design optimization process is hindered by the enormous variable space. Therefore, we have been exploring high-throughput methods for screening nanoparticles for mineral flotation. Laboratory batch flotation tests are slow, and for screening purposes, need to be replaced by a technique that is smaller in scale, faster, and can be performed in a fully automated way. The results in Figure 4 suggest that the maximum diameter of a bubble attached to a nanoparticle treated mineral would be a good predictor of flotation efficiency. Ongoing work includes the development of this approach.

CONCLUSIONS

A series of polymeric nanoparticles with varying glass transition temperatures but with similar size and surface energies was compared as flotation collectors for glass beads. The major conclusions from this work are:

(1) The maximum flotation recovery of model glass beads, cleaned pentlandite mineral and nickel ore increased with decreasing particle softness, with the most dramatic effects occurring when the nanoparticle glass transition temperature was near the flotation temperature.
(2) The maximum attached bubble diameter is a sensitive indicator of the ability of nanoparticles to promote flotation.
(3) We propose softer nanoparticles have a greater contact area with the glass beads (model mineral particles) and Pn surfaces giving greater nanoparticle-mineral particle adhesion, and thus higher flotation efficiency.

ASSOCIATED CONTENT

Supporting Information

Mineral and glass bead particle size distributions and photographs of our small scale laboratory flotation apparatus. This material is available free of charge via the Internet at http://pubs.acs.org/.

AUTHOR INFORMATION

Corresponding Author

*E-mail: peltonrh@mcmaster.ca.

Notes

The authors declare no competing financial interest.

ACKNOWLEDGMENTS

We thank the Centre for Materials and Manufacturing (CMM), a division of the Ontario Centres of Excellence (OCE), in collaboration with VALE Base Metals for funding. Zongfu Dai and Manqiu Xu from Vale for much help, samples and advice. Finally, we acknowledge Dan Zhang and Stephen Jonkhans from McMaster University for preparing the nanoparticles.

REFERENCES

(1) Fuerstenau, M.; Jameson, G.; Yoon, R. The Society for Mining, Metallurgy, and Exploration: Littleton, CO, 2007.
(2) Yang, S.; Pelton, R. H.; Raegen, A.; Montgomery, M.; Dalnoki-Veress, K. *Langmuir* **2011**, *27*, 10438−10446.
(3) Yang, S.; Pelton, R. H. *Langmuir* **2011**, *27*, 11409−11415.
(4) Yang, S.; Pelton, R.; Montgomery, M.; Cui, Y. *ACS Appl. Mater. Interfaces* **2012**, *4*, 4882−4890.
(5) Lyadov, V. V.; Gryanko, V. I.; Nikitin, I. N.; Prebobrazhenskii, B. P. *Coke Chem.* **1979**, *9*, 12.
(6) Zhan, Y. *Latices as Flocculants in Selective Flocculation of Mineral Suspensions*; University of British Columbia: Vancouver, Canada, 1999.
(7) Palmes, J. R. Effect of the Properties of Coal Surface and Flocculant Type on the Flocculation of Fine Coal. *Ph.D. Thesis*, University of British Columbia, Vancouver, Canada, 1996.
(8) Laskowski, J. S.; Yu, Z.; Zhan, Y. Hydrophobic Agglomeration of Fine Coal. In *Proceedings of the 1st UBC-McGill Bi-Annual International Symposium on Fundamentals of Mineral Processing*; Laskowski, J. S., Poling, G. W., Eds.; Metal Society of CIM: Vancouver, Canada, 1995; p 245.
(9) Palmes, J. R.; Laskowski, J. S. *Miner. Metall. Proc.* **1993**, 218−222.
(10) Attia, Y.; Yu, S. *Langmuir* **1991**, *7*, 2203−2207.
(11) Littlefair, M. J.; Lowe, N. R. S. *Int. J. Miner. Process.* **1986**, *17*, 187−203.
(12) Laskowski, J. S.; Yu, Z. *Int. J. Miner. Process.* **2000**, *58*, 237−252.
(13) Goodwin, J. W.; Ottewill, R. H.; Pelton, R. *Colloid Polym. Sci.* **1979**, *257*, 61−69.
(14) Dai, Z.; Bos, J. A.; Quinn, P.; Lee, A.; Xu, M. Flowsheet Development for Thompson Ultramafic Low-Grade Nickel Ores. In *Advances in Mineral Processing Science and Technology, 48th Annual Conference of Metallurgists of CIM*; Sudbury, Ontario, Aug 23−26, 2009 ; Gomez, C. O., Nesset, J. E., Rao, S. R., Eds.; Canadian Institute of Minining, Metallurgy and Petroleum: Westmount, Quebec, Canada, 2009; pp 217−228.
(15) Yang, S., Pelton, R., Xu, M., Dai, Z. In Nanoparticle Flotation Collectors for Pentlandite. In *Proceedings of the 44th Annual Canadian Mineral Processors Conference*; Ottawa, Ontario, Jan 17−19, 2012 ; Canadian Mineral Processors: Ottawa, Ontario, 2012; pp 225−236.
(16) Nguyen, A. V.; Schulze, H. J.; Ralston, J. *Int. J. Miner. Process.* **1997**, *51*, 183−195.
(17) Frye, G. C.; Berg, J. C. *J. Colloid Interface Sci.* **1989**, *127*, 222−238.
(18) Pelton, R. *J. Indust. Microbiol. Biotechnol.* **2002**, *29*, 149−154.
(19) Garrett, P. R. *Defoaming: Theory and Industrial Applications*; CRC Press: Boca Raton, FL, 1993; Vol. *45*.
(20) Dahneke, B. *J. Colloid Interface Sci.* **1972**, *40*, 1−13.
(21) Unertl, W. N. *Langmuir* **1998**, *14*, 2201−2207.
(22) Engqvist, C.; Forsberg, S.; Norgren, M.; Edlund, H.; Andreasson, B.; Karlsson, O. *Colloids Surf., A* **2007**, *302*, 197−203.
(23) Tomas, J. *Chem. Eng. Sci.* **2007**, *62*, 1997−2010.

(24) Wu, S. *Polymer Interface and Adhesion*; Marcel Dekker: New York, 1982.
(25) Kendall, K. *Molecular Adhesion and Its Applications: The Sticky Universe*; Plenum Press: London, 2001.
(26) Berg, J. C. *An Introduction to Interfaces and Colloids: The Bridge to Nanoscience*; World Scientific: Hackensack, NJ, 2010.
(27) Assemi, S.; Nalaskowski, J.; Johnson, W. P. *Colloids Surf., A* **2006**, *286*, 70−77.